Paleoceanography and Paleoclimatology

RESEARCH ARTICLE
10.1029/2020PA003969

Key Points:
- Micron-scale geochemical variability within modern *N. pachyderma* shells is compared to the hydrographic conditions
- We propose a new Mg/Ca to temperature relationship for *N. pachyderma* lamellar calcite
- The sensitivity of *N. pachyderma* $\delta^{18}O$ to temperature and salinity is the same in both lamellar and crust calcite

Supporting Information:
- Table S1
- Table S2
- Data Set S1
- Data Set S2
- Data Set S3
- Data Set S4
- Data Set S5
- Data Set S6
- Data Set S7
- Data Set S8
- Data Set S9
- Data Set S10

Correspondence to:
C. M. Livsey,
cmlivsey@ucdavis.edu

Citation:
Livsey, C. M., Kozdon, R., Bauch, D., Brummer, G.-J. A., Jonkers, L., Orland, I., et al. (2020). High-resolution Mg/Ca and $\delta^{18}O$ patterns in modern *Neogloboquadrina pachyderma* from the Fram Strait and Irminger Sea. *Paleoceanography and Paleoclimatology*, *35*, e2020PA003969. https://doi.org/10.1029/2020PA003969

Received 29 APR 2020
Accepted 7 AUG 2020
Accepted article online 17 AUG 2020

High-Resolution Mg/Ca and $\delta^{18}O$ Patterns in Modern *Neogloboquadrina pachyderma* From the Fram Strait and Irminger Sea

Caitlin M. Livsey[1], Reinhard Kozdon[2], Dorothea Bauch[4,5], Geert-Jan A. Brummer[6], Lukas Jonkers[3], Ian Orland[7,8], Tessa M. Hill[1], and Howard J. Spero[1]

[1]Department of Earth and Planetary Sciences, University of California, Davis, CA, USA, [2]Lamont–Doherty Earth Observatory, Columbia University, Palisades, NY, USA, [3]MARUM, Universität Bremen, Bremen, Germany, [4]GEOMAR Helmholtz Centre for Ocean Research, Kiel, Germany, [5]Leibniz Laboratory for Radiometric Dating and Stable Isotope Research, Kiel University, Kiel, Germany, [6]NIOZ, Royal Netherlands Institute for Sea Research, Department of Ocean Systems, and Utrecht University, Texel, The Netherlands, [7]WiscSIMS, Department of Geoscience, University of Wisconsin-Madison, Madison, WI, USA, [8]Wisconsin Geological and Natural History Survey, University of Wisconsin-Madison, Madison, WI, USA

Abstract *Neogloboquadrina pachyderma* is the dominant species of planktonic foraminifera found in polar waters and is therefore invaluable for paleoceanographic studies of the high latitudes. However, the geochemistry of this species is complicated due to the development of a thick calcite crust in its final growth stage and at greater depths within the water column. We analyzed the in situ Mg/Ca and $\delta^{18}O$ in discrete calcite zones using laser ablation-inductively coupled plasma-mass spectrometry, electron probe microanalysis, and secondary ion mass spectrometry within modern *N. pachyderma* shells from the highly dynamic Fram Strait and the seasonally isothermal/isohaline Irminger Sea. Here we compare shell geochemistry to the measured temperature, salinity, and $\delta^{18}O_{sw}$ in which the shells calcified to better understand the controls on *N. pachyderma* geochemical heterogeneity. We present a relationship between Mg/Ca and temperature in *N. pachyderma* lamellar calcite that is significantly different than published equations for shells that contained both crust and lamellar calcite. We also document highly variable secondary ion mass spectrometry $\delta^{18}O$ results (up to a 3.3‰ range in single shells) on plankton tow samples which we hypothesize is due to the granular texture of shell walls. Finally, we document that the $\delta^{18}O$ of the crust and lamellar calcite of *N. pachyderma* from an isothermal/isohaline environment are indistinguishable from each other, indicating that shifts in *N. pachyderma* $\delta^{18}O$ are primarily controlled by changes in environmental temperature and/or salinity rather than differences in the sensitivities of the two calcite types to environmental conditions.

1. Introduction

Numerous paleoceanographic proxies have been developed that utilize the trace element and stable isotope compositions of the calcium carbonate shells of planktonic foraminifera (e.g., Allen & Hönisch, 2012; Emiliani, 1955; Emiliani et al., 1961; Epstein et al., 1953; Hönisch et al., 2011, 2013; Kucera, 2007; Lea et al., 1999; Nürnberg et al., 1996; Ravelo & Hillaire-Marcel, 2007; Urey, 1948; Zeebe et al., 2008). Traditionally, geochemical analyses on planktonic foraminifera have pooled multiple shells and analyzed them together to obtain a single geochemical data point. However, studies on single foraminifera shells reveal that there is significant intrashell geochemical heterogeneity in chamber walls that may be due to environmental, biological, or diagenetic factors (Duckworth, 1977; Eggins et al., 2003, 2004; Fehrenbacher & Martin, 2010; Fehrenbacher et al., 2015, 2017; Jonkers et al., 2012; Kozdon et al., 2009; Sadekov et al., 2010; Spero et al., 2015; Vetter, Kozdon, et al., 2013; Wu & Hillaire-Marcel, 1994). These micron-scale variations in chamber wall geochemistry can be measured in foraminifera using different methods, including laser ablation-inductively coupled plasma-mass spectrometry (LA-ICP-MS) for trace elements and secondary ion mass spectrometry (SIMS) for stable isotopes such as $\delta^{18}O$. Combining trace element and $\delta^{18}O$ values from discrete domains of calcite within individual foraminifera has the potential to provide linked paleoceanographic information from exceptionally small samples (e.g., Vetter et al., 2017). The combination of such

high-resolution analyses on distinct domains of calcite from specific depths potentially greatly expands our capacity to reconstruct past water column hydrography on a scale that was not previously possible.

Neogloboquadrina pachyderma (sinistral-coiling) is the only polar species of planktonic foraminifera and dominates high-latitude assemblages (Bauch et al., 1997) and is therefore the primary species used to study the paleoceanography of polar regions. The exact depth habitat of *N. pachyderma* varies greatly by location and is likely controlled by the vertical temperature and chlorophyll concentration gradients (e.g., Greco et al., 2019; Jonkers & Kučera, 2017). For most of its ontogeny, *N. pachyderma* dwells near the surface where it secretes chambers composed of $CaCO_3$ that is commonly referred to as lamellar calcite (LC) (Erez, 2003; Reiss, 1957). Prior to the completion of its life cycle, *N. pachyderma* sinks through the mixed layer/upper pycnocline, and it adds a thick $CaCO_3$ crust that envelops the finer-grained LC (Arikawa, 1983; Carstens & Wefer, 1992; Kohfeld et al., 1996; Simstich et al., 2003). Assuming that the geochemistries of these two calcite domains reflect the chemistry of the water in which they were precipitated, single shell chamber walls could record hydrographic information from both the near-surface and the deeper pycnocline (Kozdon et al., 2009; Vetter, Spero, et al., 2013). Because shell [Mg] varies predominantly with temperature (Lea et al., 1999; Nürnberg, 1995) and shell $\delta^{18}O$ is modified by temperature and $\delta^{18}O_{seawater}$ ($\delta^{18}O_{sw}$; which varies with salinity and local hydrology), populations of individually analyzed *N. pachyderma* shells hold the potential to reconstruct temperature and salinity/$\delta^{18}O_{sw}$ with depth in the polar oceans.

However, while high-resolution geochemical analysis on *N. pachyderma* has the potential to revolutionize high-latitude paleoceanography, there are a number of outstanding questions that need to be addressed. First, the presence of calcite grown at different depths complicates precise interpretation of *N. pachyderma* whole shell geochemical analyses, as the ratio of crust to LC differs between individuals (Arikawa, 1983; Kohfeld et al., 1996; Kozdon et al., 2009; Simstich et al., 2003; Stangeew, 2001). Furthermore, the relationship between the geochemistry of the shell and the hydrologic conditions in which the crust and the LC precipitate, respectively, may be different (Bolton & Marr, 2013; Davis et al., 2017; Jonkers et al., 2010; Kozdon et al., 2009). Consequently, the relationships between water temperature and shell Mg/Ca and $\delta^{18}O_{calcite}$ need to be evaluated separately for *N. pachyderma* lamellar and crust calcite in order to accurately interpret geochemical data from individual shell analyses.

Here we address these outstanding questions on modern *N. pachyderma* from the Fram Strait and the Irminger Sea. The Fram Strait is the only deep-water connection between the Arctic and North Atlantic Ocean and, therefore, is the channel through which the majority of Arctic water exchange occurs (Zweng et al., 2018), contributing to the formation of North Atlantic Deep Water (Bryan, 1986). At subsurface depths of 50–200 m (Cokelet et al., 2008), warm/salty Atlantic water enters the Arctic via the West Spitsbergen Current (>2°C, >35 psu), while cold and low salinity surface water leaves the Arctic via the East Greenland Current (0–2°C, 33–34.4 psu; Consolaro et al., 2018). The movement of diverse water masses through the Fram Strait results in significant temperature and salinity gradients within and across the channel. Therefore, the Fram Strait is an ideal location to explore potential relationships between the geochemistry of *N. pachyderma* and the hydrological conditions in which the calcite was precipitated. For comparison with the Fram Strait samples, we have also analyzed *N. pachyderma* shells collected from the Irminger Sea that calcified in an isothermal and isohaline water column to evaluate the nonenvironmental controls influencing the geochemistry of the two calcite domains in a shell. Starting in January, convective mixing to >400 m depth in the central Irminger Sea produces a vertical gradient of <0.5°C and <0.3 psu (de Jong et al., 2012). Because the crust and LC for these shells grew under identical hydrologic conditions, neither geochemical variability within the shell or systematic differences between the two domains can be attributed to temperature, salinity, or $\delta^{18}O_{sw}$ changes.

In this study, we report results of in situ analyses of the geochemistry of *N. pachyderma* lamellar and crust calcite Mg/Ca using LA-ICP-MS and electron probe microanalysis (EPMA), as well as $\delta^{18}O_{calcite}$ data measured using SIMS. In addition, we conducted whole shell $\delta^{18}O_{calcite}$ analyses using standard isotope ratio mass spectrometry (IRMS) on single or pooled shells from both study sites. Hydrographic measurements (i.e., temperature, salinity, and $\delta^{18}O$) of the water in which the samples were collected are utilized to better understand the relationships between the geochemistry of the crust and lamellar domains of *N. pachyderma* and the environmental conditions during foraminiferal growth.

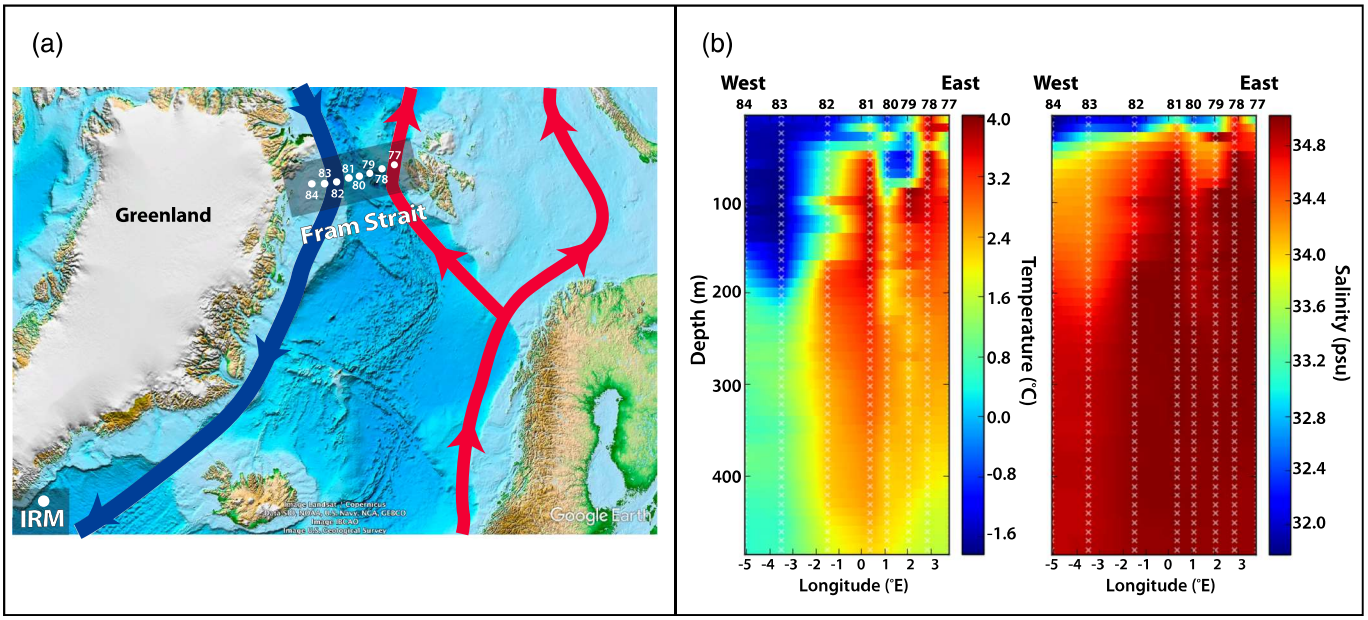

Figure 1. (a) Map of the study area with the two study areas outlined by gray rectangles. The eight stations across the Fram Strait are represented by white dots and labeled with their station number. The sediment traps from the Irminger Sea are denoted by a single white dot. (b) West-East cross sections of the Fram Strait study transect colored by temperature (°C; left) and by salinity (psu; right) to 500 m depth. Temperature and salinity measurements were collected at each of the stations every 10 m in the *z* direction (each white x represents a measurement) with interpolated results in between. *X* axis is longitude (°E) on the bottom and station # on the top.

2. Materials and Methods

2.1. Sample Collection

2.1.1. Fram Strait

Living planktonic foraminifera were collected in the Fram Strait using a vertical Hydrobios multinet tow with a 63 μm mesh from the Polarstern ARK XV/2 cruise during the summer of 1999. At each of the eight stations (Figure 1a), tows were taken from 0–50, 50–100, 100–200, 200–300, and 300–500 m depths. Onboard sample treatment and initial foraminifera picking methods were previously described by Stangeew (2001) and consisted of conserving the plankton tow collected samples in 90% denatured ethanol and storage at 4°C. Samples used in this study were *N. pachyderma* that were living at the time of capture as indicated by Rose-Bengal staining. Following the cruise, stained foraminifera were picked from the >63 μm tow samples, rinsed in distilled water, dried at room temperature, and transferred to micropaleontology slides (complete sample list and station can be found in supporting information Table S1). Water samples were collected at each of the stations using a CTD rosette at 0, 25, 50, 100, 200, 300, 400, and 500 m depths, while temperature and salinity measurements were recorded every 10 m (Figure 1b). The water samples were later analyzed for $\delta^{18}O_{sw}$, $\delta^{13}C_{DIC}$, and nutrient concentrations (Stangeew, 2001).

2.1.2. Irminger Sea

Details of the sediment trap design and deployment information in the Irminger Sea are described in Jonkers et al. (2010). These sediment traps (~2,750 m depth) were sampled every 16 days, and all samples used in this study were collected during the month of April (2006 or 2007) when the water column displayed isothermal/isohaline characteristics (Jonkers et al., 2010). Before the collection bottles were deployed in the traps, they were filled with ambient seawater, poisoned with $HgCl_2$, and buffered with Borax. Upon recovery, the bottles were kept at 4°C until samples could be processed and stored dry. Eight shells from trap IRM-3 (Sample A-14) and 12 shells from trap IRM-4 (Sample A-15) were picked from the dried 150–250 μm size fraction for subsequent analyses.

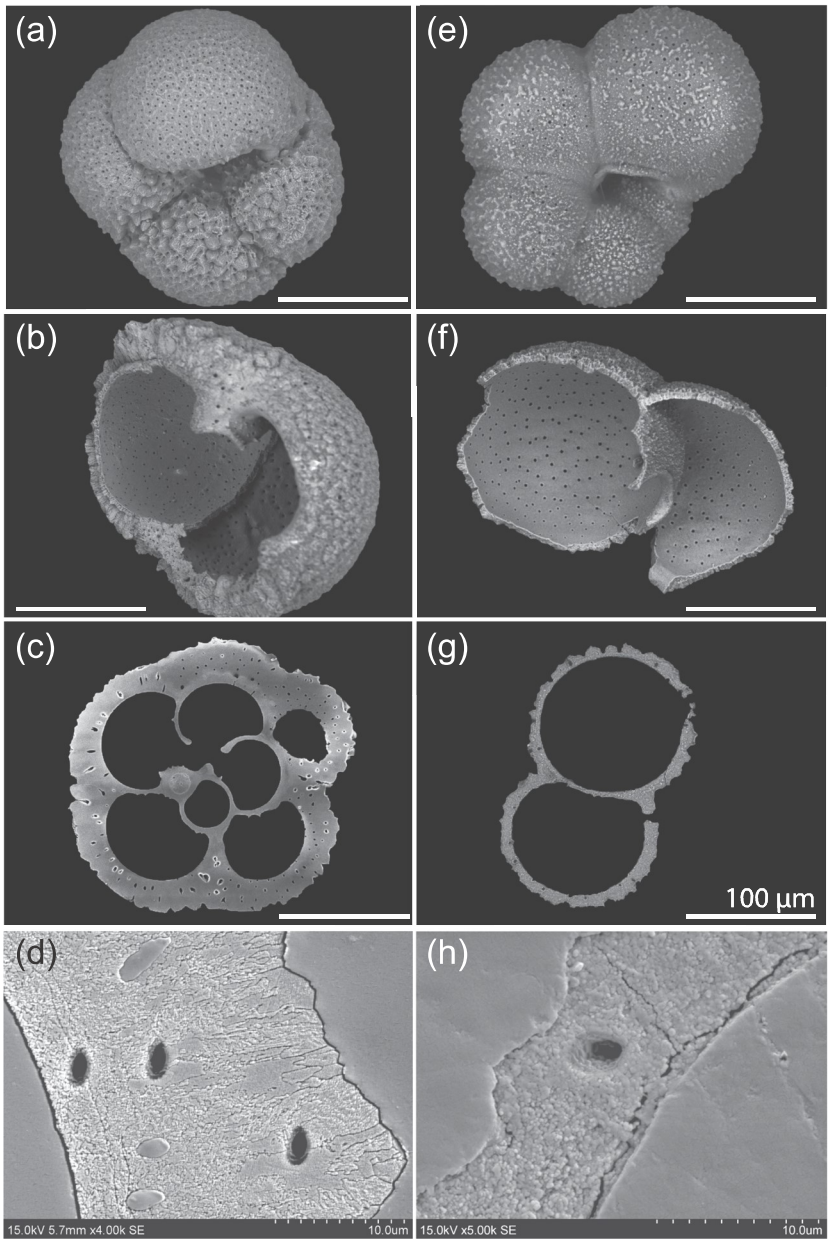

Figure 2. SEM images comparing crusted and uncrusted *N. pachyderma* shells in various stages of analysis to demonstrate differences in morphology and shell wall thickness. Tests in (a)–(d) are fully crusted shells from an Irminger Sea sediment trap, while those in (e)–(h) contain uncrusted shells collected across the Fram Strait. Shown are (a, e) whole cleaned shells, (b, f) amputated shell fragments, and (c, d, g, and h) polished cross sections of shells in an epoxy mount. In (b)–(d), the lamellar calcite can be seen as the thin inner layers that has been surrounded by the crust calcite. The difference in texture of the calcite between the two groups of shells is most apparent in (d) and (h) and is consistent across the samples (see supporting information for all SEMs). The Irminger Sea shells are smoother with evident interlocking calcite crystals and growth layers. The Fram Strait shells calcite appears more granular with higher porosity and less obvious structure to the shell walls. Scale bar is 100 µm in (a)–(d) and (e)–(g) and 10 µm in (d) and (h).

2.2. Sample Preparation

For LA-ICP-MS and SIMS analyses, individual *N. pachyderma* were picked, cracked into multiple fragments using a scalpel, and cleaned to remove remnant organics using an oxidative 1:1 solution of 35% H_2O_2:0.1 N NaOH in conjunction with eight rinses in methanol and three rounds of 30 s in methanol while in an ultrasonic bath (Mashiotta et al., 1999). Between each rinsing step, the methanol is aspirated using a pipette. This

Table 1
LA-ICP-MS Operating Procedures and Data Reduction Parameters

ICPMS: Agilent 7700x	Data reduction: LAtools
RF Power: 1350 W	Despiking data: exponential decay and signal smoothing
Argon (carrier) gas flow: 0.95–1.0 L/min	
Ar coolant gas flow: 15 L/min	Background correction: 1-D interpolation
Ar auxiliary gas flow: 1 L/min	Calibration: NIST 610-612-614
Dwell time per mass: 20–40 ms	Internal standard: 43Ca
Total sweep time: 240 s	Filters: Mn/Ca and Al/Ca < 0.5 nmol/mol
Laser-ablation system: UV Excimer Laser	
Energy density (fluence): 0.87–1.44 J/cm^2	
He gas flow: 1.05 L/min	
Laser repetition rate: 5 Hz	
Laser spot size: 40 μm square spot	
ThO+/Th+: <0.4%	

cleaning procedure is sufficiently rigorous to remove organic contamination while avoiding physical breakage of the shells or dissolution of the fragile calcite layers. After cleaning, *N. pachyderma* fragments (>50 μm surface area) were mounted on carbon tape and imaged in variable pressure mode using a Hitachi TM300 scanning electron microscope (SEM) in the UC Davis Department of Earth and Planetary Sciences. The resultant images were reviewed to assess shell microstructure and to note the orientation of the shells for subsequent analyses. Figure 2 illustrates shells from the Irminger Sea (panels a–d) and Fram Strait (panels e–h) foraminifera shells at various stages of processing and sample preparation.

2.3. LA-ICP-MS Analyses and Data Processing

Typically two LA-ICP-MS spots from 40 uncrusted shells mounted on carbon tape from the Fram Strait plankton tows ($n = 84$ spots) and 20 crusted shells from the Irminger Sea sediment traps ($n = 48$ spots) were obtained to quantify domain-specific metal/Ca profiles through shell walls. The resulting data come from shells that were collected in the 0–50, 50–100, and 100–200 m depth tows at each of the eight stations across the Fram Strait and from the IRM-4 and IRM-3 sediment trap samples. *N. pachyderma* fragments were analyzed for Me/Ca trace elements (^{11}B, ^{24}Mg, ^{25}Mg, ^{27}Al, ^{43}Ca, ^{44}Ca, ^{55}Mn, and ^{56}Ba) by ablating from the interior of the shell wall to the exterior using a Photon Machines pulsed 193 nm ArF UV excimer laser with a HelEx dual-volume sample chamber attached to an Agilent 7700x Quadrupole ICP-MS at the UC Davis Stable Isotope Laboratory in the Department of Earth and Planetary Sciences. Square 40 × 40 μm spots were ablated using a repetition rate of 5 Hz and a fluence of 0.87 J/cm^2 to generate replicate profiles from each shell while acquiring enough material to measure multiple elements simultaneously. LA-ICP-MS spot locations were chosen preferentially on areas of the F or F-1 chambers that were oriented perpendicular to the laser beam. Complete analytical settings are summarized in Table 1.

The data collected by the LA-ICP-MS system was reduced using the LAtools software package (specific settings shown in Table 1; Branson et al., 2019). Data reduction included removal of abnormal spikes/noise from ablation profiles, identifying and excluding the background counts, and applying a background correction to the data calculated using a 1-D interpolation. Sensitivity drift was accounted for using counts on NIST glass standards 610, 612, and 614 during each analytical session, which were used to generate and subsequently apply a time-sensitive calibration calculation and standardization to absolute concentration in LAtools. Elemental counts were normalized to ^{43}Ca counts, and contaminated domains were filtered out using Mn/Ca or Al/Ca concentrations above 0.5 mmol/mol (Pena et al., 2008). For each LA-ICP-MS spot, Mg/Ca profiles through the shell wall (inside to the outside) are plotted against ablation time (seconds) to reveal the internal pattern of Mg/Ca variability (all laser profiles raw preprocessed laser data and the LAtools minimal export files can be found in the supporting information).

2.4. Oxygen Isotope Analyses

LA-ICP-MS ablated fragments were removed from the carbon tape using ethanol and mounted for $\delta^{18}O_{calcite}$ analyses with a CAMECA IMS 1280 SIMS at the WiscSIMS Laboratory, University of Wisconsin, Madison. Fragments were arranged based on size and placed within 5 mm of the center of a 1 in. diameter circular

Table 2
Summary of Measured $\delta^{18}O_{calcite}$ (‰ VPDB) of Plankton Tow Collected N. pachyderma Lamellar Calcite at Various Depths at Each of the Eight Stations Across the Fram Strait

Station	Collection depth (m)	Average SIMS $\delta^{18}O$ calcite (‰ VPDB ±2SE)	# shells (# of spots)	IRMS $\delta^{18}O$ calcite (‰ VPDB)	# shells	△ $\delta^{18}O$ calcite SIMS-IRMS (‰ VPDB)	IRMS δ18Ocalcite (‰ VPDB ± 2SE) from Stangeew (2001)	# samples	Measured $\delta^{18}O$ water (‰ VSMOW)
77	50–100	−0.36 (±0.73)	2 (12)	—	—	—	2.39	1	0.25
77	100–200	−0.57 (±0.93)	2 (4)	—	—	—	2.42 (±0.15)	3	0.2
78	50–100	−0.6	1 (1)	2.16	5	−2.76	2.67 (±0.44)	3	0.27
78	100–200	0.06 (±0.37)	2 (9)	2.73	6	−2.67	2.8 (±0.05)	4	0.28
79	0–50	—	—	3.45	8	—	3.33 (±0.06)	3	0.86
79	50–100	—	—	—	—	—	2.8 (±0.38)	3	0.07
79	100–200	−0.5 (±3.33	1 (2)	2.66	6	−3.16	2.83 (±0.22)	5	0.29
80	0–50	—	—	—	—	—	3.15 (±0.40)	3	0.14
80	50–100	0.96 (±0.96)	2 (6)	—	—	—	—	—	0.15
80	100–200	−0.17 (±0.72)	2 (4)	3.27	5	−3.44	3.29 (±0.08)	3	0.25
81	0–50	—	—	—	—	—	2.54 (±0.73)	3	0.15
81	50–100	−0.21 (±1.22)	2 (4)	—	—	—	2.98 (±0.47)	4	0.29
81	100–200	0.78 (±0.42)	2 (9)	2.62	5	−1.84	2.60 (±0.22)	6	0.23
82	0–50	—		3.03	4	—	3.07 (±0.14)	3	−0.07
82	50–100	—	—	3.57	6	—	3.14 (±0.23)	3	0.06
82	100–200	0.99 (±0.81)	1 (5)	3.2	5	−2.21	3.26 (±0.13)	3	0.17
83	0–50	—	—	2.71	5	—	1.68 (±0.19)	3	−1.67
83	50–100	−1.03 (±0.84)	2 (3)	—	—	—	2.58 (±0.15)	6	−0.79
83	100–200	0.58 (±0.30)	2 (4)	3.41	8	−2.83	2.84 (±0.1)	8	−0.23
84	0–50	—	—	—	—	—	2.33 (±0.27)	2	−1.97
84	50–100	0.27 (±0.69)	2 (5)	—	—	—	2.56 (±0.1)	2	−0.85
84	100–200	0.33 (±0.26)	2 (8)	3.22	6	−2.89	2.95 (±0.07)	6	−0.2

Note. Stations 77 and 78 did not have significant shells in the shallowest tows (0–50 m) and therefore do not have any $\delta^{18}O_{calcite}$ results from those depths. The average $\delta^{18}O_{calcite}$ (‰ VPDB) measured on the SIMS and the IRMS are shown with the difference between the two averaged measurements to demonstrate the offset between the two analytical techniques. Also shown is the $\delta^{18}O_{water}$ (‰VSMOW) measured on water samples collected concurrent with the plankton tows.

mold along with two grains of the WiscSIMS calcite standard UWC-3 ($\delta^{18}O$ = +12.49‰ VSMOW or −17.17‰ VPDB; Kozdon et al., 2009). Samples were cast in Buehler EpoxiCure resin under vacuum and subsequently polished to expose cross sections of the shell walls close to regions that were analyzed by LA-ICP-MS. Images of the polished shells were generated with SEM BSE to qualitatively determine the thickness of exposed shell walls and cross section geometry prior to analysis (see Figures 2c and 2g and all remaining SEMs in the supporting information). Immediately before analysis, the epoxy mounts were cleaned with ethanol and DI-water, dried in a vacuum oven, and gold coated. Between one and seven spots within the LC of each shell was analyzed for $\delta^{18}O$ using a 3 μm diameter $^{133}Cs^{+}$ beam with analytical settings and conditions similar to those described in Kozdon et al. (2009). After every ~tenth SIMS spot analysis, UWC-3 calcite standard was measured four times to bracket the samples to correct for instrumental mass fractionation. No additional correction was made for instrumental drift.

Reproducibility of the individual spot analyses of UWC-3 standard (bracketing samples) is assigned as precision (reproducibility) of unknown samples. Average precision for all 19 brackets of 3 micron spots is ±0.77‰ (2*SD*); reproducibility (2*SD*) of UWC-3 in individual brackets varied from 0.37‰ to 1.43‰ with only three brackets >1.0‰ (Table S2). The bracketing standards and sample $\delta^{18}O$ data were finally corrected and converted from VSMOW to VPDB using the conversion of Coplen et al. (1983). All subsequent ‰ values presented are reported on the VPDB scale. After SIMS analysis, the sample mounts were imaged by SEM BSE, and all SIMS spots were screened postanalysis to ensure that only calcite was measured and to exclude data from "irregular pits" (Cavosie et al., 2005; Linzmeier et al., 2016). Furthermore, the secondary ion yield and background corrected $^{16}OH/^{16}O$ ratios reported relative to bracketing standards from all analyses were examined to identify any anomalous data that should be removed (Wycech, Kelly, Kitajima, et al., 2018). Anomalous results were removed and are not included in any data tables or supporting information.

Additional Fram Strait plankton tow shells were oxidatively cleaned, roasted at 375°C in vacuo for 35 min to remove remnant carbon tape, and then run on an Optima IRMS in the Stable Isotope Lab at UC Davis. In

order to obtain masses large enough to be analyzed on the IRMS (8–15 μg), three to six individual foraminifera from the same sample were combined and run together. Due to shortage of specimens in some Fram Strait tow depth samples, some samples contain a mix of individuals from adjacent collection depths at the same site to obtain sufficient mass for IRMS analyses. This information is described for each sample in Table 2.

2.5. Electron Microprobe Analyses

In preparation for analysis on the electron microprobe, SIMS sample mounts containing the Fram Strait samples were gently repolished to remove the gold coat and then recoated with carbon. Mg and Ca elemental maps were generated on the mounted samples with a Cameca SX-100 electron microprobe in the UC Davis Department of Earth and Planetary Sciences. Elemental maps were produced using 15 keV voltage, 15 nA beam current, a 1 μm spot size rasterized over the area of each shell, and a dwell time of 1 s. Mg and Ca counts were collected concurrently, and resultant Mg/Ca (counts/counts) maps were generated in RStudio. Each shell fragment was analyzed, mapped, and then colored using the RStudio color palette "topo.colors." For all mounts, spots with Ca counts below 1,000 could not be distinguished from background and were therefore masked. All EPMA maps (Figure 3 and supporting information) are shown at a 1 pixel per μm resolution with each color scale specific to that respective shell. EPMA counts were not converted to mmol/mol since no internal standardization was done at the time of analysis, and all shells were previously analyzed via LA-ICP-MS, so further quantification was not needed.

3. Results

3.1. Fram Strait Lamellar Mg/Ca

All LA-ICP-MS profiles from 40 individual shells from the Fram Strait were combined to determine the LC Mg/Ca to temperature relationship. The total range of mean shell lamellar Mg/Ca among the shells is 0.58 to 4.77 (±1.28 2SE) mmol/mol. In addition to large intershell variability, the Mg/Ca ratios within single shells (individual profiles through shells) also vary significantly, with intrashell ranges between 3 and 4 mmol/mol. The interspot variability between Mg/Ca profiles within single shells is smaller, with 2*SD* ranging from 0–2.08 mmol/mol with an average of 1.07 mmol/mol (Table S3). Intrashell values from here on will refer to the Mg/Ca values through shell walls.

The mean shell Mg/Ca ratios are compared to the average CTD measured temperatures at the water depths from which the samples were collected, which include 21 different water temperatures ranging from −1.81°C to 3.80°C (Figure 4 and Table S3). While it is possible that shells were advected to the sample location, it is unlikely that any of the individual foraminifera originated from a completely different water mass, and therefore, the CTD measured temperatures are interpreted to reflect the conditions in which the shells grew. Figure 4 shows the relationship between average LA-ICP-MS Mg/Ca data from individual shell LC and the ambient temperatures recorded at the plankton tow collection depths assuming in situ calcification. From these data, we obtain the exponential relationship (preexponential and exponential statistics are ±2σ standard error):

$$\mathrm{Mg/Ca\ (mmol/mol)} = 1.95\ (\pm 0.08) * e^{(0.082(\pm 0.03)*T)} \quad (1)$$

Though a linear model was comparable to the exponential fit, we follow established protocol and adhere to the law of thermodynamics to apply an exponential relationship. The precision of temperature reconstructions (±2σ) is calculated by inputting the range of measured Mg/Ca into Equation 1 using the upper and lower 95% confidence constraints on the coefficients. The resulting precision using this relationship for the calibrated temperature range is ±0.44°C.

Overall, the samples from the Fram Strait plankton tows appeared to lack an outer crust layer, and therefore, we interpret that shell wall geochemical analyses were only conducted on LC. The presence of low Mg/Ca ratios (1–2 mmol/mol) on the outer portions of some shell walls indicate that some of the shells may display early crusting (Figure 3). These low Mg/Ca domains are evident in both the LA-ICP-MS profiles and the microprobe Mg/Ca maps and vary in thickness both between chambers and individuals (e.g., Specimens PT1a and PT20a). The presence of alternating high and low Mg/Ca bands is apparent in the tow-collected shells, with thicker shells revealing a larger number of bands. Broadly, shells display a trend from higher

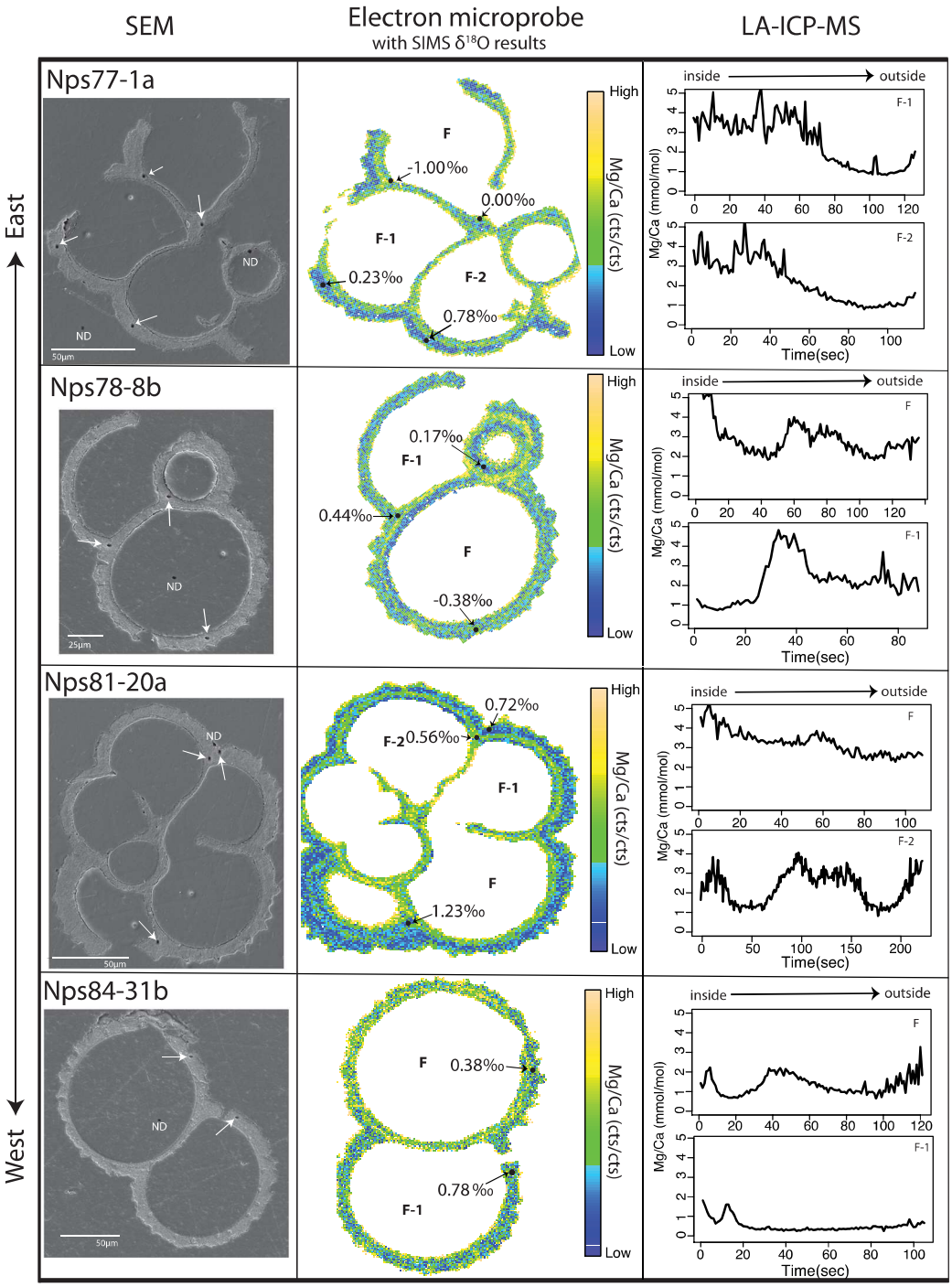

Figure 3. Compilation of geochemical results for four shells (PT1a, PT8b, PT20a, and PT31b) spanning the longitudinal transect in the Fram Strait from East to West (top to bottom). The left column shows SEM BSE images with SIMS pits (white arrows). Spots on the shells or surrounding epoxy that resemble SIMS pits but did not yield any $\delta^{18}O$ data are labeled "ND" for "no data." The middle column contains EPMA-generated Mg/Ca maps with a unique scale (counts/counts) for each shell and measured SIMS $\delta^{18}O$ values (‰VPDB; black arrows). Chambers are labeled by their relationship to the final (F) chamber. On the right are measured LA-ICP-MS Mg/Ca (mmol/mol) profiles for two spots through the shell fragments. All profiles were taken from the inside of a shell to the outside.

Mg/Ca in the LC of the inner shell walls to lower Mg/Ca toward the outer surfaces, with at least one prominent low-Mg/Ca band closer to the inside edge of the shell (Figure 3).

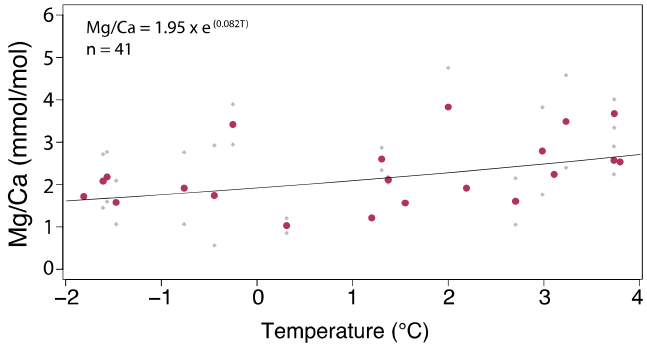

Figure 4. LA-ICP-MS Mg/Ca (mmol/mol) versus temperature (°C) results from the lamellar calcite in individual Fram Strait *N. pachyderma* shells (small gray diamonds) with the average Mg/Ca value at each recorded temperature (solid circles). Each diamond is the average Mg/Ca ratio for all ablation profiles through an individual shell. The solid circles represent the arithmetic mean Mg/Ca from all profiles that were analyzed at that temperature. Exponential regression (Equation 1) is through the individual shell values (small gray diamonds).

3.2. Mg/Ca and $\delta^{18}O$ From Irminger Sea Lamellar and Crust Calcite

Because the fully crusted *N. pachyderma* samples obtained from the Irminger Sea very likely grew in a well-mixed water column that lacked temperature or salinity variation, the shell geochemistry should not have been affected by variations in these parameters. Individual shells exhibit intershell and intrashell Mg/Ca variations, with an average range of 0.35 mmol/mol within single ablation profiles (Table S4), which is markedly less variable relative to the Fram Strait samples. Interspot variability in these shells was very low as well with an average range of 0.30 mmol/mol (Table S4). The patterns within the laser profiles indicate lower Mg/Ca in the crust calcite of the individual shells supporting the microprobe results of Jonkers et al. (2016), although the crust and LC Mg/Ca differ by <0.5 mmol/mol (Figure 5a and supporting information). For all the samples, Mg/Ca profiles through the lamellar and crust calcites of Irminger Sea shells reveal a total range of mean Mg/Ca of 0.70 to 1.95 mmol/mol. Overall, the Irminger Sea Mg/Ca results support the observations that Mg incorporation into *N. pachyderma* calcite differs between the crust and LCs (Davis et al., 2017; Hendry et al., 2009; Jonkers et al., 2013; Steinhardt et al., 2015), but the difference is small, and the lower variability and general agreement of Mg/Ca at a population scale indicate that temperature is the dominant control over *N. pachyderma* Mg/Ca.

To assess how $\delta^{18}O_{calcite}$ varies between the lamellar and crust calcite in the Irminger Sea samples, 79 SIMS spots were analyzed on 16 of the shells targeted by LA-ICP-MS in the preceding paragraph (Figure 5b). Thirty-six SIMS spots were located within the LC region of the shells, while the remaining analyses were located within the crust calcite (see SEM images in the supporting information). The difference between the average measured $\delta^{18}O_{calcite}$ on the crust versus LC is 0.18‰, and a paired *t* test reveals that the crust and LC $\delta^{18}O_{calcite}$ values are statistically similar ($p < 0.05$), demonstrating that a single temperature versus $\delta^{18}O_{calcite}$ relationship can be used to interpret shell $\delta^{18}O$ geochemistry. Mean spot-to-spot precision (2*SD*) for these data is ±0.72‰ for all analyses (Tables S2 and S5). Notably, the previously reported IRMS $\delta^{18}O_{calcite}$ values for shells from the same sediment trap samples were 2.31‰ for IRM-3 A-14 and 2.52‰ for IRM-4 A-15 (Figure 5b; Jonkers et al., 2010) suggesting *N. pachyderma* displays an IRMS-SIMS $\delta^{18}O$ offset of ~0.7‰ similar to that previously documented in other planktonic foraminifera species (Wycech, Kelly, Kozdon, et al., 2018).

3.3. SIMS and IRMS $\delta^{18}O$ From Fram Strait LC

For the Fram Strait plankton tow samples, 75 SIMS $\delta^{18}O$ spots were analyzed from the 25 thickest shells (Figure 6 and Tables S2 and S6). Depending on the surface area of exposed shell wall, individuals were analyzed 1–7 times using an ~3 μm spot diameter. The average $\delta^{18}O$ of the LC for each individual foraminifera was 1.5‰, with the largest $\delta^{18}O$ range within a single shell of 3.3‰ (Table S6). The average analytical precision for each SIMS analysis was 0.64‰ (2*SD*) which is considerably lower than the intrashell $\delta^{18}O_{calcite}$ range, indicating that the intrashell range exceeds analytical precision by a factor of 2.5–5. All raw data collected on the SIMS are presented in Table S2. SIMS $\delta^{18}O_{calcite}$ data are plotted on EPMA Mg/Ca maps with adjacent LA-ICP-MS Mg/Ca profiles in Figure 3. The SEM images in the first column of Figure 3 identify the SIMS pits location on the microprobe maps. The intrashell $\delta^{18}O$ variability does not correlate with chamber number or distance along the shell wall, indicating that the $\delta^{18}O_{calcite}$ variability is not easily explained by ontogeny (Figure 3). Across the 25 *N. pachyderma* shells analyzed by SIMS, the $\delta^{18}O_{calcite}$ values of individual shells range from −2.7‰ to +2.4‰, with average shell values between −1.3‰ and 1.8‰ (Figure 6 and Table S6). Compared to the spot-to-spot precision (2*SD*), the geochemical variability between shells cannot be explained by analytical uncertainty alone.

IRMS analyses conducted on pooled Fram Strait *N. pachyderma* shells yield $\delta^{18}O_{calcite}$ values that are offset from the SIMS $\delta^{18}O_{calcite}$ data collected from the same group of shells (Table 2 and Figure 6). The IRMS

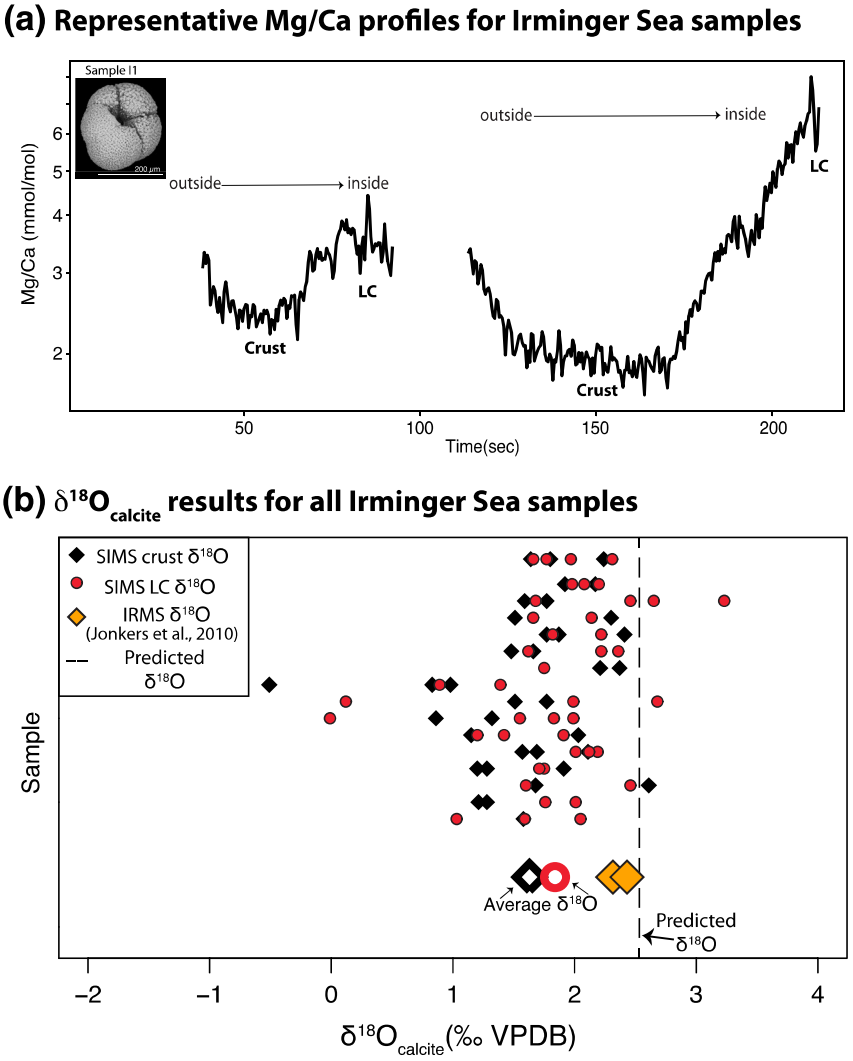

Figure 5. (a) Two representative LA-ICP-MS Mg/Ca (mmol/mol) profiles through a single *N. pachyderma* shell fragment from the Irminger Sea with the crust and lamellar calcite domains labeled (Sample I1). (b) Plot of Irminger Sea sediment trap collected *N. pachyderma* $\delta^{18}O_{calcite}$ results. SIMS $\delta^{18}O_{calcite}$ (‰VPDB) data shown in red circles (lamellar calcite) and black diamonds (crust calcite). Average $\delta^{18}O_{calcite}$ (‰VPDB) for all spots within the lamellar and crust calcites are shown in larger hollow symbols below the individual results. Published IRMS results on pooled shells shown are in orange diamonds (Jonkers et al., 2010), and predicted $\delta^{18}O_{calcite}$ (‰VPDB) for the water column is denoted by a vertical line.

$\delta^{18}O_{calcite}$ values are 1.84‰ to 3.44‰ higher than the average SIMS $\delta^{18}O_{calcite}$ in the tows. Figure 6 shows the Fram Strait SIMS and IRMS data plotted with predicted calcite $\delta^{18}O$ values from Kim and O'Neil (1997) based on measured temperature, $\delta^{18}O_{sw}$, and salinity at each site. The SIMS $\delta^{18}O$ spots exclusively show more negative $\delta^{18}O$ compared to both predicted and IRMS-derived $\delta^{18}O$ and do not appear to show any consistent patterns with depth at each station. The IRMS $\delta^{18}O$ results agree well with predicted $\delta^{18}O$ at the same depth, with an average offset of 0.32 ± 0.79‰. Furthermore, the samples that show the largest spread in IRMS $\delta^{18}O$ values coincide with a region of the water column where the hydrology and, therefore, the predicted $\delta^{18}O$ are complicated.

3.4. Evaluation of Calcite Microstructure

SEM micrographs of the shells from the Fram Strait plankton tows and the Irminger Sea sediment traps reveal distinct calcite fabrics between the two set of samples (Figure 2). A comparison between crusted

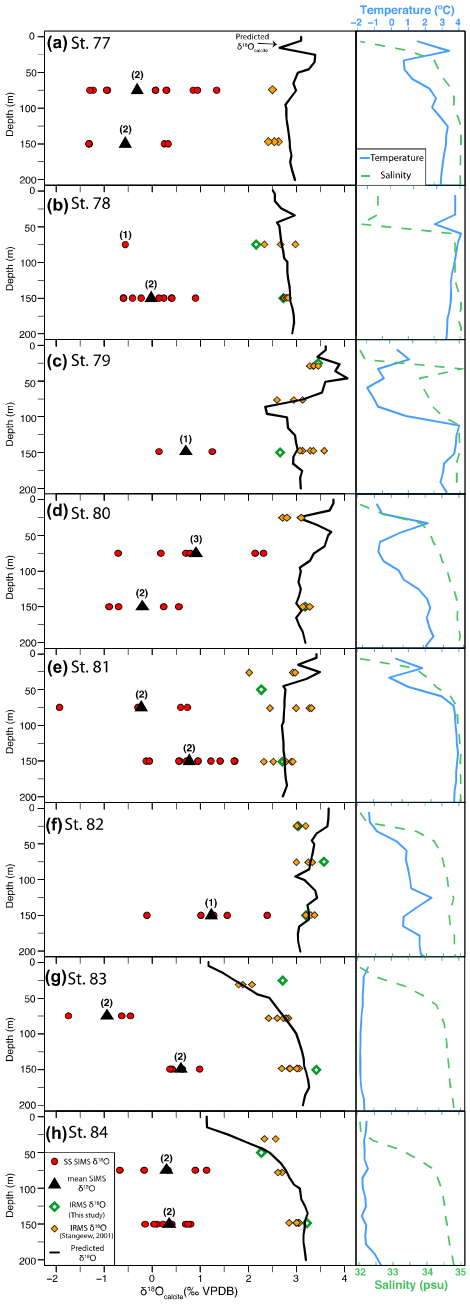

Figure 6. (a–h) Composite of plankton tow collected *N. pachyderma* $\delta^{18}O_{calcite}$ (‰VPDB) results (left) alongside the CTD measured temperature and salinity (right) for the upper 200 m for the eight stations (77–84) from East to West across the Fram Strait. $\delta^{18}O_{calcite}$ (‰VPDB) results from SIMS analysis are shown as individual spots (SS) in red circles and the average of all shells from given station/depth in black triangles. The "*n*" indicated is the total number of shells included in the averaged value. IRMS $\delta^{18}O_{calcite}$ (‰VPDB) results on pooled shells are shown in green hollow diamonds with published IRMS $\delta^{18}O_{calcite}$ results from the same tows shown in orange solid diamonds (Stangeew, 2001). All $\delta^{18}O_{calcite}$ data are plotted at the average depths of their respective tows (more details in Table 2). The predicted $\delta^{18}O_{calcite}$ (‰) for each station (solid black line) was calculated using the paleotemperature equation from Kim and O'Neil (1997) with the CTD measured temperature and $\delta^{18}O_w$ from 0–200 m.

and noncrusted *N. pachyderma* shells from the Irminger Sea and the Fram Strait, respectively, are shown in Figure 2 as whole shells (panels a and e), cracked fragments (panels b and f), and polished cross sections (panels c, d, g, and h). The bottom SEM micrographs show cross sections of the two shells, in which the Irminger Sea shell displays a smoother, denser, more homogenous and compact calcite surface compared to the shell from the Fram Strait. Figure 3 also contains photomicrographs of cross-sectioned shells from the Fram Strait revealing irregular surfaces, apparent enhanced porosity, and overall rough or mottled textures.

4. Discussion

4.1. Mg/Ca Patterns in *N. pachyderma*

LC in the Fram Strait plankton tow *N. pachyderma* examined here display distinctive patterns within single shells and between shells. Both LA-ICP-MS and microprobe results reveal that LC shells contain multiple high/low Mg bands with lower Mg/Ca ratios toward the outside surfaces of some of the chambers (Figure 3). These patterns are consistent with Mg/Ca profiles reported from the shell walls in other nonsymbiont-bearing planktonic foraminifera such as *Globorotalia inflata*, *G. scitula*, *G. tumida*, *G. menardii*, *G. truncatulinoides*, *Neogloboquadrina incompta*, and *Pulleniatina obliquiloculata* (Davis et al., 2017; Hathorne et al., 2003, 2009; Kunioka et al., 2006; Sadekov et al., 2005; Steinhardt et al., 2015). While the microprobe maps highlight subtle differences in Mg/Ca patterns between chambers in the Fram Strait samples, the LA-ICP-MS results demonstrate that when the closely spaced Mg bands are averaged, *N. pachyderma* LC Mg/Ca is relatively constant between different spots in individual shells (Table S3). This result indicates that while there are still controls on *N. pachyderma* Mg/Ca, the mean LC Mg/Ca of a population of shells can be used to estimate environmental temperature (Figure 4 and Equation 1).

The Mg/Ca ratios in crusted single *N. pachyderma* shells from the Irminger Sea ranged between 0.70 and 1.95 ($\pm$0.54 2*SD*) mmol/mol with the lowest Mg/Ca in the outer crust region of the shell walls. These data agree with the EPMA-generated Mg maps on samples from the same sediment traps (Jonkers et al., 2016). Although these *N. pachyderma* shells calcified in an isothermal water column in the Irminger Sea, they exhibit distinctly zoned Mg/Ca ratios (Figure 5a), supporting the conclusions of others (Davis et al., 2017; Jonkers et al., 2016) that Mg/Ca banding and crust/LC Mg content in *N. pachyderma* is controlled by foraminifera physiology and is a part of the chamber formation process. The exact mechanism controlling the Mg concentration within *N. pachyderma* (and other species) is not fully understood and requires further investigation. Homogeneous low Mg/Ca calcite was also reported for *N. incompta* crust relative to LC from NE Pacific specimens grown in the laboratory (Davis et al., 2017). Although a thick crust was not observed in the plankton tow specimens we analyzed from the Fram Strait, a few *N. pachyderma* shells (see PT1a and PT20a in Figure 3) display considerably reduced Mg/Ca ratios in the outer surfaces of some chamber walls which may represent early crust calcite precipitation in these upper water column-collected specimens.

Table 3
Published Mg/Ca Versus Temperature Relationships for Neogloboquadrina pachyderma

Reference	Equation	Temperature range (°C)	Sample type	Sample location
Jonkers et al. (2013)	Mg/Ca = 0.60 * e^(0.09 * T)	5–10	Sediment trap	Irminger Sea
Kozdon et al. (2009)	Mg/Ca = 0.13 * T + 0.35	3–6	Core top	Norwegian Sea
Nürnberg (1995)	Mg/Ca = 0.41 * e^(0.083 * T)	0–15	Core top	Norwegian Sea
Vàzquez Riveiros et al. (2016)	Mg/Ca = 0.58 * e^(0.084 * T)	−1–9	Core top	Southern Ocean
This study (Equation 2)	Mg/Ca = 0.93 * e^(0.086 * T)	−2–12	Plankton tow and cultured specimens	Fram Strait and Bodega Bay, CA

A number of Mg/Ca versus temperature calibrations have been published for *N. pachyderma* from core top and sediment trap samples (Table 3). Although these relationships were generated using whole *N. pachyderma* shells that contained both lamellar and crust calcite, the mass of calcite analyzed was dominated by the low Mg crusts. *N. pachyderma* crust is estimated to range between 50% and 80% of the total test mass, therefore making a correction based on the relative proportion of LC to crust difficult (Arikawa, 1983; Kohfeld et al., 1996; Kozdon et al., 2009; Stangeew, 2001). Despite averaging high and low Mg bands for each specimen, the Mg/Ca versus temperature sensitivity of our Fram Strait LC relationship (Equation 1), 7.5% per °C, is similar to published calibrations for whole shells (Figure 7a). However, the preexponential constant is considerably larger because of the lack of low-Mg crusts in these samples (Figure 7a) resulting in Equation 1 plotting well above other published calibrations for this species.

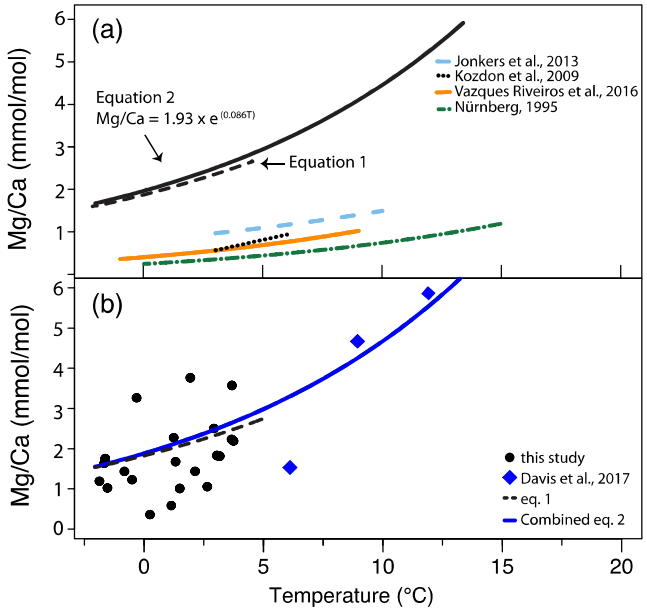

Figure 7. (a) Plot of published *N. pachyderma* Mg/Ca (mmol/mol) versus temperature (°C) relationships labeled with their corresponding references (Table 3) alongside the relationship generated from data collected in this study (Equation 1) and the combined relationship with the 9°C and 12°C data from Davis et al. (2017; Equation 2; see discussion for details). All relationships extend throughout the temperature range in which they were calibrated. (b) Average Mg/Ca values at each recorded temperature from the Fram Strait (black spots; same data as the solid circles in Figure 4) with Equation 1 (dashed line). Blue diamonds are data from cultured *N. pachyderma* at 6°C, 9°C, and 12°C from Davis et al. (2017) with combined Equation 2 (solid blue line). The large difference between Equations 1 and 2 and the published equations is due to the low-Mg crust calcite dominating the signal in the latter equations.

Since Equation 1 was calculated at low temperatures (−1.81°C to 3.80°C), the precision on the relationship is below the precision of the instruments, and therefore, it is necessary to combine our data with similar data from warmer temperatures. Davis et al. (2017) conducted temperature experiments on living *N. pachyderma* collected in the NE Pacific off the coast of California and presented a Mg/Ca versus temperature calibration for *N. pachyderma* LC between 6–12°C (n = 10 shells). Figure 7b compares the Davis et al. (2017) Mg/Ca data with the average shell Mg/Ca from our Fram Strait plankton tow data and Equation 1. We cannot explain why the 6°C data point (n = 4 shells) from Davis et al. (2017) falls below the LC data set but note that this sample's ratio agrees with the Mg/Ca of whole *N. pachyderma* shells which contain both crust and LC. Because crusting has been proposed to initiate at temperatures below 8–10°C in nonspinose foraminifera (Hemleben et al., 1985), we speculate that one or more of the four cultured shells analyzed in this sample contained crust calcite which would have reduced the Mg/Ca ratio of the entire sample. If we omit the 6°C data point from the combined data set, we obtain

$$\mathrm{Mg/Ca\ (mmol/mol)} = 1.93\ (\pm 0.04) * e^{(0.086(\pm 0.13) * T)} \quad (2)$$

which is nearly indistinguishable from Equation 1. This combined equation has a precision ($\pm 2\sigma$) of ±1.97°C at the typically cooler temperatures in the Arctic Ocean.

This suggests that we can potentially use this equation to calculate the temperature of the waters in which the foraminifera were living in from the measurements of the Mg/Ca ratios of *N. pachyderma* LC. The consistency between our *N. pachyderma* LC-only Mg/Ca versus temperature relationship and those for other species of planktonic foraminifera indicate that while whole shell Mg/Ca versus temperature reconstructions are not applicable for this species, we can now utilize *N. pachyderma* LC to refine high-latitude paleotemperature

records. However, the large spread in Mg/Ca values and the inconsistent patterns within shell walls, it is likely that a larger sample size may be necessary to detect minor changes in temperature. That said, our results suggest that if the crust Mg/Ca versus temperature relationship can be determined, *N. pachyderma* lamellar and crust calcite can be used to independently compute water column temperature profiles during different phases of shell formation.

4.2. Irminger Sea Sediment Trap *N. pachyderma* $\delta^{18}O$

Lamellar and crust calcite from single *N. pachyderma* shells from the isothermal and isohaline Irminger Sea yield overlapping SIMS $\delta^{18}O$ values that are indistinguishable from each other (Figure 5b). The distribution of the $\delta^{18}O_{calcite}$ values in these shells indicates that the $^{18}O/^{16}O$ ratio of crust and LC are affected equally by equilibrium fractionation offsets due to vital effects, carbonate ion effects, temperature, and $\delta^{18}O_{sw}$ (Pearson, 2012). This result supports the use of a single relationship to reconstruct water column temperature and salinity from intrashell $\delta^{18}O_{calcite}$ variability in the fossil record (Kozdon et al., 2009) and indicate that the mechanism responsible for the observable shift in Mg/Ca between the LC and the crust does not similarly affect the $\delta^{18}O$. Furthermore, these results support the conclusions of Kozdon et al. (2009) that the distinct crust and LC $\delta^{18}O$ values observed in fossil *N. pachyderma* are likely due to calcification in different regions of the water column with different temperature/$\delta^{18}O_{sw}$ properties rather than a change in fractionation with crust formation. Finally, we suggest that the reason different species-specific paleotemperature equations have been proposed for whole shell *N. pachyderma* data is due to the mixing of LC and crust calcite phases that precipitated in water with different temperature and salinity conditions (Duplessy et al., 1981; Kohfeld et al., 1996).

Averaged SIMS measurements of shell $\delta^{18}O_{calcite}$ were significantly lower than previously published measurements on these samples using an IRMS ($\Delta\delta^{18}O_{SIMS\text{-}IRMS} = -0.7 \pm 1.18$‰; Jonkers et al., 2010). A comparable $\Delta\delta^{18}O_{SIMS\text{-}IRMS}$ offset to that observed in these *N. pachyderma* data was reported in a study of another planktonic foraminifera, *Orbulina universa*. Wycech, Kelly, Kozdon, et al. (2018) reported an offset of −0.9‰ between SIMS and IRMS $\delta^{18}O_{calcite}$ values based on analyses of chamber wall fragments from multiple shells. The similarity in the $\Delta\delta^{18}O_{SIMS\text{-}IRMS}$ offsets suggests the magnitude of the offset is broadly applicable to SIMS analyses on modern foraminifera shells, and this type of careful species-specific test will improve comparisons of SIMS and IRMS data in future analyses. Potential factors contributing to this $\Delta\delta^{18}O_{SIMS\text{-}IRMS}$ offset are thoroughly explored in Wycech, Kelly, Kozdon, et al. (2018, and references therein).

4.3. Fram Strait Plankton Tow *N. pachyderma* $\delta^{18}O_{calcite}$

IRMS $\delta^{18}O_{calcite}$ data from pooled tow-collected *N. pachyderma* are evaluated across the Fram Strait using the temperature, salinity, and $\delta^{18}O_{seawater}$ measurements made at each station (Table 2; Stangeew, 2001). Figure 6 presents a compilation of the measured $\delta^{18}O_{calcite}$ results for each of the eight stations across the Fram Strait shown with the corresponding temperature and salinity profiles for the upper 200 m of the water column. Predicted $\delta^{18}O_{calcite}$ values for *N. pachyderma* were generated using temperature and measured or salinity-calculated $\delta^{18}O_{seawater}$ with the relationship of Kim and O'Neil (1997). Predicted $\delta^{18}O_{calcite}$ for the six eastern stations (Stations 77–82; Figures 6a–6f) utilize measured $\delta^{18}O_{seawater}$ values rather than salinity-based $\delta^{18}O_{seawater}$ values because sea ice melt had a significant influence on $\delta^{18}O_{water}$ and salinity at these stations (Stangeew, 2001). Figure 6 includes previously published IRMS-generated $\delta^{18}O_{calcite}$ data from the same *N. pachyderma* tow material analyzed shortly after the cruise (Stangeew, 2001; Table 2 and Figure 6). The IRMS data from Stangeew (2001) are indistinguishable from the IRMS results obtained in this study, and the $\delta^{18}O$ data are in good agreement with predicted $\delta^{18}O_{calcite}$ at each station. We observe an average $\Delta\delta^{18}O_{measured\text{-}predicted}$ offset of 0.38 ± 0.5‰ for the IRMS data ($\Delta\delta^{18}O$ offset range of 0.02‰ to 1.03‰). These data demonstrate that *N. pachyderma* LC $\delta^{18}O$ does not deviate significantly from predicted $\delta^{18}O_{calcite}$ and confirms our assumption that these tow-collected *N. pachyderma* are recording ambient conditions at each collection site.

Intrashell and interchamber $\delta^{18}O_{calcite}$ was assessed in the LC using SIMS (Figures 3 and 6). These data reveal significant LC wall $\delta^{18}O_{calcite}$ variations and a clear $\delta^{18}O_{calcite}$ offset compared to the IRMS data. Figure 6 shows that the SIMS $\delta^{18}O_{calcite}$ measurements display an average LC offset of −2.91‰ (±1.9‰)

from the predicted $\delta^{18}O_{calcite}$ values. This offset and shell wall variability does not correlate with Mg/Ca banding or growth layers (Figure 3) and is not consistent across shells. There is no straightforward explanation for these data. Kozdon et al. (2009) presented a similar range of SIMS $\delta^{18}O_{calcite}$ data from *N. pachyderma* LC in plankton tow collected shells from the Eastern Nordic Seas that show a progressive $\delta^{18}O_{calcite}$ increase toward the lamellar-crust boundary. In their study, average $\delta^{18}O_{calcite}$ was ~3‰ higher in the crust relative to the LC. The interchamber $\delta^{18}O_{calcite}$ variation in the shells walls of Fram Strait *N. pachyderma* does not appear to correlate with distance from inside of the shell but rather varies randomly within shells.

SIMS $\delta^{18}O_{calcite}$ data have been collected from the shell walls of other species of planktonic foraminifera using 10 μm spots, which has an analysis area 11× greater than the 3 μm spot used here (Kozdon et al., 2011, 2013; Vetter, Spero, et al., 2013; Wycech, Kelly, Kitajima, et al., 2018, Wycech, Kelly, Kozdon, et al., 2018). These studies show intrashell variation of <1‰, with variations exceeding this level explained by diagenesis or gametogenic calcification. Although increased measurement variance is expected with a smaller SIMS spot size, we did not observe this in 3 μm spot SIMS analyses of LC and calcite crust on the Irminger Sea *N. pachyderma* shells. Rather, crusted *N. pachyderma* shells from the Irminger Sea display $\delta^{18}O$ variance similar to that reported in other studies (i.e., Kozdon et al., 2009; Valley & Kita, 2009; Vetter, Spero, et al., 2013), with an offset of 0.7‰ from IRMS data that was previously reported in other species (Figure 5b; Wycech, Kelly, Kozdon, et al., 2018). Hence, the variation of SIMS $\delta^{18}O_{calcite}$ in Fram Strait samples and the large $\delta^{18}O$ offset from the IRMS measurements on the same material are not likely due to SIMS spot size. Postprocessing of the SIMS $\delta^{18}O$ data does not provide further insight. Simultaneous measurements of $^{16}OH/^{16}O$—a qualitative indicator of H-bearing inclusions (e.g., water or organic material)—are similar between samples in this study. No abnormalities were noted in the secondary ion count rates or relative yield (Table S2) of Fram Strait sample analyses. Furthermore, measurements of standard calcite are comparable between all of the analytical sessions (Table S2), indicating that the IRMS offset and variable $\delta^{18}O$ of Fram Strait samples must be caused by a characteristic unique to those shells.

4.4. Potential Factors Contributing to Variability in SIMS Results on Plankton Tow *N. pachyderma*

The most obvious difference between the Fram Strait plankton tow *N. pachyderma* and the Irminger Sea sediment trap shells is the texture or fabric of the polished shell walls that were analyzed by SIMS (Figure 2). Polished Fram Strait plankton tow shells display a clear granular texture in the microfabric of the chamber wall, whereas the polished surfaces of the Irminger Sea *N. pachyderma* shells are smooth without texture. For precise and accurate SIMS analyses, it is prerequisite that the standard closely matches the sample with respect to mineralogy, crystal structure, and trace/minor elemental composition (Valley & Kita, 2009). The *N. pachyderma* shells from plankton tows feature an apparent porous texture, in contrast with the smooth and homogenous texture of the marble standard. Though the texture of the plankton tow shells appear porous, the consistency in the count rate on the SIMS indicates that the data cannot be explained by void space. Rather, we postulate that the granular texture negatively affects the precision and accuracy of the SIMS $\delta^{18}O_{calcite}$ measurements of the Fram Strait plankton tow samples. Possible sources of the porous texture observed in the plankton tow samples could be a result of sample treatment/preparation or a shift in calcification causing modification of shell microstructure with ontogeny. The former includes increased proportion of organics retained within the shell walls resulting in postcollection dissolution of calcite, dissolution caused by storage in ethanol, physical erosion of thin calcite walls during polishing, or a combination of these factors.

5. Conclusions

We have analyzed Mg/Ca and $\delta^{18}O$ in single *N. pachyderma* shells from plankton tows deployed in the Fram Strait and a sediment trap from the Irminger Sea to investigate the geochemical patterns within and between shells to assess the utility of this species in paleoceanographic reconstructions. We combined Mg/Ca and $\delta^{18}O$ analyses on discrete domains within shells using LA-ICP-MS, EPMA, and SIMS and were able to directly compare geochemical variability with micron-scale resolution. Hydrographic information that was measured concurrently with the collection of foraminifera allowed us to directly interpret the foraminiferal geochemistry in an environmental context. The plankton tow samples were collected along a transect

across the Fram Strait, which exhibits large ranges in temperature, salinity, and $\delta^{18}O_{sw}$ allowing us to compare shell geochemistries across a relatively large environmental gradient. These data were compared and supplemented by sediment trap samples from the seasonally isothermal and isohaline Irminger Sea in order to disentangle changes in temperature and salinity from biological or physiological factors. Our conclusions are as follows:

1. LC in *N. pachyderma* Mg/Ca can potentially be used to calculate paleotemperatures using Equation 2 defined in this study. This relationship is significantly different from published equations using whole shells likely due to the low-Mg crust diluting the signal in whole shell measurements.
2. LA-ICP-MS and EPMA results on plankton tow samples indicate that Mg/Ca banding is present in the LC of *N. pachyderma*, while the LA-ICP-MS profiles on crusted sediment trap samples support previous observations that *N. pachyderma* crust calcite contains low Mg/Ca even in the absence of temperature variability.
3. The agreement in LC and crust SIMS $\delta^{18}O_{calcite}$ data in trap-caught samples from the isothermal/isohaline Irminger Sea reveals that the source of the low Mg/Ca in *N. pachyderma* crust does not similarly influence the $\delta^{18}O$.
4. The −0.7‰ offset between IRMS and SIMS $\delta^{18}O_{calcite}$ on the Irminger Sea samples supports previous studies comparing these two analytical techniques and indicates that this offset correction should be applied to SIMS $\delta^{18}O_{calcite}$ on Holocene foraminiferal calcite.
5. The SIMS $\delta^{18}O_{calcite}$ results from the LC of the Fram Strait plankton tow samples are quite variable and significantly more negative compared to the IRMS analyses on the same samples. IRMS $\delta^{18}O$ results on these shells agree with predicted $\delta^{18}O_{calcite}$ calculated using the $\delta^{18}O_{seawater}$ and salinity profiles from the sampling location.
6. The granular microtexture of the Fram Strait plankton tow samples, in contrast to the Irminger Sea samples and the crystalline standard, could have degraded the precision and accuracy of the SIMS $\delta^{18}O_{calcite}$ results in those shells.

Overall, our results suggest that *N. pachyderma* shells remain a powerful proxy carrier for paleoceanographic reconstructions in the high latitudes, with the acknowledgement of a few outstanding considerations. As such, the LC-specific Mg/Ca to temperature relationship is a definite improvement over previous whole-shell equations as it excludes the low-Mg crust calcite, which has a different relationship between Mg/Ca and temperature. In terms of using the Mg/Ca ratio of *N. pachyderma* crust calcite to reconstruct temperatures at depth, the potential of deriving a Mg/Ca to temperature calibration may prove difficult as the mechanism controlling the homogenously low-Mg crust calcite remains unknown. Regarding the controls on $\delta^{18}O_{calcite}$ in *N. pachyderma*, this study reveals that IRMS-analyzed shells produce $\delta^{18}O$ values consistent with predicted $\delta^{18}O$ based on the temperature and $\delta^{18}O_{sw}$ using the paleotemperature equation of Kim and O'Neil (1997), while SIMS-analyzed shells produce an offset of −0.7‰. Furthermore, SIMS $\delta^{18}O$ analyses on crusted shells from the isothermal/isohaline Irminger Sea reveal that there is no difference between the lamellar and crust calcites, and therefore, the crust and LC likely do not require distinct calibration relationships with respect to $\delta^{18}O$. Finally, the variable and imprecise SIMS $\delta^{18}O$ results on highly irregular and granular plankton tow shells indicate that the texture of shells might have a great impact on SIMS $\delta^{18}O$ results and therefore should be carefully examined to avoid inaccurate interpretations.

Acknowledgments

This research was funded by NSF Award OCE-1550041 (R. K. and H. J. S.) and support from the UC Davis Earth and Planetary Sciences Durrell Fund (C. L.). We thank Nick Botto for his assistance with the electron microprobe analyses, Greg Baxter for thin section sample preparation for the SIMS analyses, Bill Schneider for facilitation with the UW SEM, and Noriko Kita, Mike Spicuzza, and John Valley for assistance at WiscSIMS. WiscSIMS is supported by NSF Award EAR-1658823 and the University of Wisconsin-Madison.

Data Availability Statement

All data produced from this study are archived in the Arctic Data Center repository in the National Science Foundation (https://doi.org/10.18739/A2319S316, https://doi.org/10.18739/A26T0GW55) and the paleoclimatology dataset repository in the National Centers for Environmental Information, NOAA database (https://www.ncdc.noaa.gov/paleo/study/28250, https://www.ncdc.noaa.gov/paleo/study/28270).

References

Allen, K. A., & Hönisch, B. (2012). The planktic foraminiferal B/Ca proxy for seawater carbonate chemistry: A critical evaluation. *Earth and Planetary Science Letters*, *345*, 203–211.

Arikawa, R. (1983). Distribution and taxonomy of *Globigerina pachyderma* (Ehrenberg) off the Sanriku coast, Northeast Honshu, Japan (*Globoquadrina dutertrei*). *Science Reports - Tohoku University, Second Series: Geology*, *53*(2), 103–157.

Bauch, D., Carstens, J., & Wefer, G. (1997). Oxygen isotope composition of living *Neogloboquadrina pachyderma* (sin.) in the Arctic Ocean. *Earth and Planetary Science Letters*, *146*(1–2), 47–58. https://doi.org/10.1016/S0012-821X(96)00211-7

Bolton, A., & Marr, J. P. (2013). Trace element variability in crust-bearing and non crust-bearing *Neogloboquadrina incompta*, P-D intergrade and *Globoconella inflata* from the Southwest Pacific Ocean: Potential paleoceanographic implications. *Marine Micropaleontology*, *100*, 21–33. https://doi.org/10.1016/j.marmicro.2013.03.008

Branson, O., Fehrenbacher, J. S., Vetter, L., Sadekov, A. Y., Eggins, S. M., & Spero, H. J. (2019). LAtools: A data analysis package for the reproducible reduction of LA-ICPMS data. *Chemical Geology*, *504*, 83–95. https://doi.org/10.1016/j.chemgeo.2018.10.029

Bryan, F. (1986). High-latitude salinity effects and interhemispheric thermohaline circulations. *Nature*, *323*(6086), 301–304. https://doi.org/10.1038/323301a0

Carstens, J., & Wefer, G. (1992). Recent distribution of planktonic foraminifera in the Nansen Basin, Arctic Ocean. *Deep Sea Research Part A. Oceanographic Research Papers*, *39*(2), S507–S524. https://doi.org/10.1016/S0198-0149(06)80018-X

Cavosie, A. J., Valley, J. W., & Wilde, S. A. (2005). Magmatic $\delta^{18}O$ in 4400–3900 Ma detrital zircons: A record of the alteration and recycling of crust in the Early Archean. *Earth and Planetary Science Letters*, *235*(3–4), 663–681. https://doi.org/10.1016/j.epsl.2005.04.028

Cokelet, E. D., Tervalon, N., & Bellingham, J. G. (2008). Hydrography of the West Spitsbergen Current, Svalbard Branch: Autumn 2001. *Journal of Geophysical Research*, *113*, C01006. https://doi.org/10.1029/2007JC004150

Consolaro, C., Rasmussen, T. L., & Panieri, G. (2018). Palaeoceanographic and environmental changes in the eastern Fram Strait during the last 14,000 years based on benthic and planktonic foraminifera. *Marine Micropaleontology*, *139*, 84–101. https://doi.org/10.1016/j.marmicro.2017.11.001

Coplen, T. B., Kendall, C., & Hopple, J. (1983). Comparison of stable isotope reference samples. *Nature*, *302*(5905), 236–238. https://doi.org/10.1038/302236a0

Davis, C. V., Fehrenbacher, J. S., Hill, T. M., Russell, A. D., & Spero, H. J. (2017). Relationships between temperature, pH, and crusting on Mg/Ca ratios in laboratory-grown *Neogloboquadrina* foraminifera. *Paleoceanography*, *32*, 1137–1152. https://doi.org/10.1002/2017PA003111

de Jong, M. F., van Aken, H. M., Våge, K., & Pickart, R. S. (2012). Convective mixing in the central Irminger Sea: 2002–2010. *Deep Sea Research Part I: Oceanographic Research Papers*, *63*, 36–51. https://doi.org/10.1016/j.dsr.2012.01.003

Duckworth, D. (1977). Magnesium concentration in the tests of the planktonic foraminifer *Globorotalia truncatulinoides*. *Journal of Foraminiferal Research*, *7*(4), 304–312. https://doi.org/10.2113/gsjfr.7.4.304

Duplessy, J. C., Bé, A. W. H., & Blanc, P. L. (1981). Oxygen and carbon isotopic composition and biogeographic distribution of planktonic foraminifera in the Indian Ocean. *Palaeogeography, Palaeoclimatology, Palaeoecology*, *33*(1–3), 9–46. https://doi.org/10.1016/0031-0182(81)90031-6

Eggins, S., De Deckker, P., & Marshall, J. (2003). Mg/Ca variation in planktonic foraminifera tests: Implications for reconstructing palaeo-seawater temperature and habitat migration. *Earth and Planetary Science Letters*, *212*(3–4), 291–306. https://doi.org/10.1016/S0012-821X(03)00283-8

Eggins, S. M., Sadekov, A., & De Deckker, P. (2004). Modulation and daily banding of Mg/Ca in *Orbulina universa* tests by symbiont photosynthesis and respiration: A complication for seawater thermometry? *Earth and Planetary Science Letters*, *225*(3–4), 411–419. https://doi.org/10.1016/j.epsl.2004.06.019

Emiliani, C. (1955). Pleistocene temperature variations in the Mediterranean. *The Journal of Geology*, *63*(6), 538–578. https://doi.org/10.1086/626295

Emiliani, C., Mayeda, T., & Selli, R. (1961). Paleotemperature analysis of the Plio-Pleistocene section at Le Castella, Calabria, southern Italy. *Geological Society of America Bulletin*, *72*(5), 679–688. https://doi.org/10.1130/0016-7606(1961)72[679:PAOTPS]2.0.CO;2

Epstein, S., Buchsbaum, R., Lowenstam, H. A., & Urey, H. C. (1953). Revised carbonate-water isotopic temperature scale. *GSA Bulletin*, *64*(11), 1315–1326. https://doi.org/10.1130/0016-7606(1953)64[1315:RCITS]2.0.CO;2

Erez, J. (2003). The source of ions for biomineralization in foraminifera and their implications for paleoceanographic proxies. *Reviews in Mineralogy and Geochemistry*, *54*(1), 115–149. https://doi.org/10.2113/0540115

Fehrenbacher, J., & Martin, P. (2010). Mg/Ca variability of the planktonic foraminifera *G. ruber s.s.* and *N. dutertrei* from shallow and deep cores determined by electron microprobe image mapping. *IOP Conference Series: Earth and Environmental Science, 9*, 012018.

Fehrenbacher, J. S., Russell, A. D., Davis, C. V., Gagnon, A. C., Spero, H. J., Cliff, J. B., et al. (2017). Link between light-triggered Mg-banding and chamber formation in the planktic foraminifera *Neogloboquadrina dutertrei*. *Nature Communications*, *8*, 1–10.

Fehrenbacher, J. S., Spero, H. J., Russell, A. D., Vetter, L., & Eggins, S. (2015). Optimizing LA-ICP-MS analytical procedures for elemental depth profiling of foraminifera shells. *Chemical Geology*, *407–408*, 2–9.

Greco, M., Jonkers, L., Kretschmer, K., Bijma, J., & Kucera, M. (2019). Depth habitat of the planktonic foraminifera *Neogloboquadrina pachyderma* in the northern high latitudes explained by sea-ice and chlorophyll concentrations. *Biogeosciences*, *16*(17), 3425–3437. https://doi.org/10.5194/bg-16-3425-2019

Hathorne, E. C., Alard, O., James, R. H., & Rogers, N. W. (2003). Determination of intratest variability of trace elements in foraminifera by laser ablation inductively coupled plasma-mass spectrometry. *Geochemistry, Geophysics, Geosystems*, *4*(12), 8408. https://doi.org/10.1029/2003GC000539

Hathorne, E. C., James, R. H., & Lampitt, R. S. (2009). Environmental versus biomineralization controls on the intratest variation in the trace element composition of the planktonic foraminifera *G. Inflata* and *G. Scitula*. *Paleoceanography*, *24*, PA4204. https://doi.org/10.1029/2009PA001742

Hemleben, C., Spindler, M., Breitinger, I., & Deuser, W. G. (1985). Field and laboratory studies on the ontogeny and ecology of some globorotaliid species from the Sargasso Sea off Bermuda. *Journal of Foraminiferal Research*, *15*(4), 254–272. https://doi.org/10.2113/gsjfr.15.4.254

Hendry, K. R., Rickaby, R. E. M., Meredith, M. P., & Elderfield, H. (2009). Controls on stable isotope and trace metal uptake in *Neogloboquadrina pachyderma* (sinistral) from an Antarctic sea-ice environment. *Earth and Planetary Science Letters*, *278*(1–2), 67–77. https://doi.org/10.1016/j.epsl.2008.11.026

Hönisch, B., Allen, K. A., Lea, D. W., Spero, H. J., Eggins, S. M., Arbuszewski, J., et al. (2013). The influence of salinity on Mg/Ca in planktic foraminifers—Evidence from cultures, core-top sediments and complementary $\delta^{18}O$. *Geochimica et Cosmochimica Acta*, *121*, 196–213. https://doi.org/10.1016/j.gca.2013.07.028

Hönisch, B., Allen, K. A., Russell, A. D., Eggins, S. M., Bijma, J., Spero, H. J., et al. (2011). Planktic foraminifers as recorders of seawater Ba/Ca. *Marine Micropaleontology*, *79*(1–2), 52–57. https://doi.org/10.1016/j.marmicro.2011.01.003

Jonkers, L., Brummer, G. J. A., Peeters, F. J. C., Van Aken, H. M., & De Jong, M. F. (2010). Seasonal stratification, shell flux, and oxygen isotope dynamics of leftcoiling *N. pachyderma* and *T. quinqueloba* in the western subpolar North Atlantic. *Paleoceanography*, *25*, PA2204. https://doi.org/10.1029/2009PA001849

Jonkers, L., Buse, B., Brummer, G. J. A., & Hall, I. R. (2016). Chamber formation leads to Mg/Ca banding in the planktonic foraminifer *Neogloboquadrina pachyderma*. *Earth and Planetary Science Letters*, *451*, 177–184. https://doi.org/10.1016/j.epsl.2016.07.030

Jonkers, L., De Nooijer, L. J., Reichart, G. J., Zahn, R., & Brummer, G. J. A. (2012). Encrustation and trace element composition of *Neogloboquadrina dutertrei* assessed from single chamber analyses—Implications for paleotemperature estimates. *Biogeosciences*, *9*(11), 4851–4860. https://doi.org/10.5194/bg-9-4851-2012

Jonkers, L., Jiménez-Amat, P., Mortyn, P. G., & Brummer, G. J. A. (2013). Seasonal Mg/Ca variability of *N. pachyderma* (s) and *G. bulloides*: Implications for seawater temperature reconstruction. *Earth and Planetary Science Letters*, *376*, 137–144. https://doi.org/10.1016/j.epsl.2013.06.019

Jonkers, L., & Kučera, M. (2017). Quantifying the effect of seasonal and vertical habitat tracking on planktonic foraminifera proxies. *Climate of the Past*, *13*(6), 573–586. https://doi.org/10.5194/cp-13-573-2017

Kim, S.-T., & O'Neil, J. (1997). Equilibrium and nonequilibrium oxygen isotope effects in synthetic carbonates. *Geochimica et Cosmochimica Acta*, *61*(16), 3461–3475.

Kohfeld, K. E., Fairbanks, R. G., Smith, S. L., & Walsh, I. D. (1996). *Neogloboquadrina pachyderma* (sinistral coiling) as paleoceanographic tracers in polar oceans: Evidence from Northeast Water Polynya plankton tows, sediment traps, and surface sediments. *Paleoceanography*, *11*(6), 679–699. https://doi.org/10.1029/96PA02617

Kozdon, R., Ushikubo, T., Kita, N. T., Spicuzza, M., & Valley, J. W. (2009). Intratest oxygen isotope variability in the planktonic foraminifer *N. pachyderma*: Real vs. apparent vital effects by ion microprobe. *Chemical Geology*, *258*(3–4), 327–337. https://doi.org/10.1016/j.chemgeo.2008.10.032

Kozdon, R., Kelly, D. C., Kita, N. T., Fournelle, J. H., & Valley, J. W. (2011). Planktonic foraminiferal oxygen isotope analysis by ion microprobe technique suggests warm tropical sea surface temperatures during the Early Paleogene. *Paleoceanography*, *26*, PA3206. https://doi.org/10.1029/2010PA002056

Kozdon, R., Kelly, D. C., Kitajima, K., Strickland, A., Fournelle, J. H., & Valley, J. W. (2013). In situ $\delta^{18}O$ and Mg/Ca analyses of diagenetic and planktic foraminiferal calcite preserved in a deep-sea record of the Paleocene-Eocene thermal maximum. *Paleoceanography*, *28*, 517–528. https://doi.org/10.1002/palo.20048

Kucera, M. (2007). Chapter six planktonic foraminifera as tracers of past oceanic environments. *Developments in Marine Geology*, *1*(07), 213–262. https://doi.org/10.1016/S1572-5480(07)01011-1

Kunioka, D., Shirai, K., Takahata, N., Sano, Y., Toyofuku, T., & Ujiie, Y. (2006). Microdistribution of Mg/Ca, Sr/Ca, and Ba/Ca ratios in *Pulleniatina obliquiloculata* test by using a NanoSIMS: Implication for the vital effect mechanism. *Geochemistry, Geophysics, Geosystems*, *7*, Q12P20. https://doi.org/10.1029/2006GC001280

Lea, D. W., Mashiotta, T. A., & Spero, H. J. (1999). Controls on magnesium and strontium uptake in planktonic foraminifera determined by live culturing. *Geochimica et Cosmochimica Acta*, *63*(16), 2369–2379. https://doi.org/10.1016/S0016-7037(99)00197-0

Linzmeier, B. J., Kozdon, R., Peters, S. E., & Valley, J. W. (2016). Oxygen isotope variability within *Nautilus* shell growth bands. *PLoS ONE*, *11*(4), 1–31.

Mashiotta, T., Lea, D. W., & Spero, H. J. (1999). Glacial-interglacial changes in subantarctic sea surface temperature and $d^{18}O$-water using foraminiferal Mg. *Earth and Planetary Science Letters*, *170*(4), 417–432. https://doi.org/10.1016/S0012-821X(99)00116-8

Nürnberg, D. (1995). Magnesium in tests of *Neogloboquadrina pachyderma* sinistral from high northern and southern latitudes. *Journal of Foraminiferal Research*, *25*(4), 350–368. https://doi.org/10.2113/gsjfr.25.4.350

Nürnberg, D., Bijma, J., & Hemleben, C. (1996). Assessing the reliability of magnesium in foraminiferal calcite as a proxy for water mass temperatures. *Geochimica et Cosmochimica Acta*, *60*(5), 803–814. https://doi.org/10.1016/0016-7037(95)00446-7

O'Neil, J., & Kim, S.-T. (1997). Equilibrium and nonequilibrium oxygen isotope effects in synthetic carbonates. *Geochimica et Cosmochimica Acta*, *61*(16), 3461–3475.

Pearson, P. N. (2012). Oxygen isotopes in foraminifera: Overview and historical review. *The Paleontological Society Papers*, *18*, 1–38. https://doi.org/10.1017/S1089332600002539

Pena, L. D., Cacho, I., Calvo, E., Pelejero, C., Eggins, S., & Sadekov, A. (2008). Characterization of contaminant phases in foraminifera carbonates by electron microprobe mapping. *Geochemistry, Geophysics, Geosystems*, *9*, Q07012. https://doi.org/10.1029/2008GC002018

Ravelo, A. C., & Hillaire-Marcel, C. (2007). Chapter eighteen the use of oxygen and carbon isotopes of foraminifera in paleoceanography. *Developments in Marine Geology*, *1*(07), 735–764. https://doi.org/10.1016/S1572-5480(07)01023-8

Reiss, Z. (1957). The Bilamellidea, nov. superfam. and remarks on Cretaceous Globorotaliids. *Contributions to Cushman Foundation Foraminiferal Research*, *8*(1), 127–145.

Sadekov, A. Y., Eggins, S. M., & De Deckker, P. (2005). Characterization of Mg/Ca distributions in planktonic foraminifera species by electron microprobe mapping. *Geochemistry, Geophysics, Geosystems*, *6*, Q12P06. https://doi.org/10.1029/2005GC000973

Sadekov, A. Y., Eggins, S. M., Klinkhammer, G. P., & Rosenthal, Y. (2010). Effects of seafloor and laboratory dissolution on the Mg/Ca composition of *Globigerinoides sacculifer* and *Orbulina universa* tests—A laser ablation ICPMS microanalysis perspective. *Earth and Planetary Science Letters*, *292*(3–4), 312–324. https://doi.org/10.1016/j.epsl.2010.01.039

Simstich, J., Sarnthein, M., & Erlenkeuser, H. (2003). Paired $\delta^{18}O$ signals of *Neogloboquadrina pachyderma* (s) and *Turborotalita quinqueloba* show thermal stratification structure in Nordic Seas. *Marine Micropaleontology*, *48*(1–2), 107–125. https://doi.org/10.1016/S0377-8398(02)00165-2

Spero, H. J., Eggins, S. M., Russell, A. D., Vetter, L., Kilburn, M. R., & Hönisch, B. (2015). Timing and mechanism for intratest Mg/Ca variability in a living planktic foraminifer. *Earth and Planetary Science Letters*, *409*, 32–42. https://doi.org/10.1016/j.epsl.2014.10.030

Stangeew, E. (2001). Distribution and isotopic composition of living planktonic foraminifera *N. pachyderma* (sinistral) and *T. quinqueloba* in the high latitude North Atlantic. Doctoral dissertation, Christian-Albrechts Universität Kiel, Germany, 1–98.

Steinhardt, J., Cléroux, C., De Nooijer, L. J., Brummer, G. J., Zahn, R., Ganssen, G., & Reichart, G. J. (2015). Reconciling single-chamber Mg/Ca with whole-shell $\delta^{18}O$ in surface to deep-dwelling planktonic foraminifera from the Mozambique Channel. *Biogeosciences*, *12*(8), 2411–2429. https://doi.org/10.5194/bg-12-2411-2015

Urey, H. C. (1948). Oxygen isotopes in nature and in the laboratory. *Science*, *108*(2810), 489–496. https://doi.org/10.1126/science.108.2810.489

Valley, J. W., & Kita, N. T. (2009). In situ oxygen isotope geochemistry by ion microprobe. *MAC Short Course: Secondary Ion Mass Spectrometry in the Earth Sciences*, *41*, 19–63.

Vàzquez Riveiros, N., Govin, A., Waelbroeck, C., Mackensen, A., Michel, E., Moreira, S., et al. (2016). Mg/Ca thermometry in planktic foraminifera: Improving paleotemperature estimations for *G. bulloides* and *N. pachyderma* left. *Geochemistry, Geophysics, Geosystems*, *17*, 1247–1566.

Vetter, L., Kozdon, R., Mora, C. I., Eggins, S. M., Valley, J. W., Hönisch, B., & Spero, H. J. (2013). Micron-scale intrashell oxygen isotope variation in cultured planktic foraminifers. *Geochimica et Cosmochimica Acta*, *107*, 267–278. https://doi.org/10.1016/j.gca.2012.12.046

Vetter, L., Spero, H. J., Eggins, S. M., Williams, C., & Flower, B. P. (2017). Oxygen isotope geochemistry of Laurentide ice-sheet meltwater across termination I. *Quaternary Science Reviews*, *178*, 102–117. https://doi.org/10.1016/j.quascirev.2017.10.007

Vetter, L., Spero, H. J., Russell, A. D., & Fehrenbacher, J. S. (2013). LA-ICP-MS depth profiling perspective on cleaning protocols for elemental analyses in planktic foraminifers. *Geochemistry, Geophysics, Geosystems*, *14*, 2916–2931. https://doi.org/10.1002/ggge.20163

Wu, G., & Hillaire-Marcel, C. (1994). Oxygen isotope compositions of sinistral *Neogloboquadrina pachyderma* tests in surface sediments: North Atlantic Ocean. *Geochimica et Cosmochimica Acta*, *58*(4), 1303–1312. https://doi.org/10.1016/0016-7037(94)90383-2

Wycech, J. B., Kelly, D. C., Kitajima, K., Kozdon, R., Orland, I. J., & Valley, J. W. (2018). Combined effects of gametogenic calcification and dissolution on $\delta^{18}O$ measurements of the planktic foraminifer *Trilobatus sacculifer*. *Geochemistry, Geophysics, Geosystems*, *19*, 4487–4501. https://doi.org/10.1029/2018GC007908

Wycech, J. B., Kelly, D. C., Kozdon, R., Orland, I. J., Spero, H. J., & Valley, J. W. (2018). Comparison of $\delta^{18}O$ analyses on individual planktic foraminifer (*Orbulina universa*) shells by SIMS and gas-source mass spectrometry. *Chemical Geology*, *483*, 119–130. https://doi.org/10.1016/j.chemgeo.2018.02.028

Zeebe, R. E., Zachos, J. C., Caldeira, K., & Tyrrell, T. (2008). Carbon emissions and acidification. *Science*, *321*(5885), 51–52. https://doi.org/10.1126/science.1159124

Zweng, M. M., Boyer, T. P., Baranova, O. K., Reagan, J. R., Seidov, D., & Smolyar, I. V. (2018). An inventory of Arctic Ocean data in the World Ocean Database. *Earth System Science Data*, *10*(1), 677–687. https://doi.org/10.5194/essd-10-677-2018